SCIENTIFIC REPORTS

OPEN

SUBJECT AREAS:
MATERIALS CHEMISTRY
INORGANIC CHEMISTRY

Received
9 January 2014

Accepted
26 March 2014

Published
14 April 2014

Correspondence and requests for materials should be addressed to K.-X.W. (k.wang@sjtu.edu.cn) or J.-S.C. (chemcj@sjtu.edu.cn)

* These authors contributed equally to this work.

In situ catalytic growth of large-area multilayered graphene/MoS_2 heterostructures

Wei Fu*, Fei-Hu Du*, Juan Su, Xin-Hao Li, Xiao Wei, Tian-Nan Ye, Kai-Xue Wang & Jie-Sheng Chen

School of Chemistry and Chemical Engineering, Shanghai Jiao Tong University, Shanghai 200240, China.

Stacking various two-dimensional atomic crystals on top of each other is a feasible approach to create unique multilayered heterostructures with desired properties. Herein for the first time, we present a controlled preparation of large-area graphene/MoS_2 heterostructures via a simple heating procedure on Mo-oleate complex coated sodium sulfate under N_2 atmosphere. Through a direct *in situ* catalytic reaction, graphene layer has been uniformly grown on the MoS_2 film formed by the reaction of Mo species with S pecies, which is from the carbothermal reduction of sodium sulfate. Due to the excellent graphene "painting" on MoS_2 atomic layers, the significantly shortened lithium ion diffusion distance and the markedly enhanced electronic conductivity, these multilayered graphene/MoS_2 heterostructures exhibit high specific capacity, unprecedented rate performance and outstanding cycling stability, especially at a high current density, when used as an anode material for lithium batteries. This work provides a simple but efficient route for the controlled fabrication of large-area multilayered graphene/metal sulfide heterostructures with promising applications in battery manufacture, electronics or catalysis.

With superb electronic and mechanical properties, two dimensional (2D) atomic crystals have shown great promise in a plethora of applications[1–7]. Efforts have been devoted to the development of atomic-scale heterostructures made from a combination of alternating layers of graphene, MoS_2, hexagonal boron-nitride and so on[8–12]. Such heterostructures provide a higher electronic quality for lateral graphene devices[13–15] and also allow for a conceptually new degree of flexibility in designing films for applications in battery manufacture, electronics or catalysis[3,16–20]. Accordingly, interest has been directed to the exploitation of reliable methods for the fabrication of large-area high-quality heterostructures[21]. So far, the most popular strategy for the preparation of atomic-scale heterostructures is based on the poly-methylmethacrylate (PMMA) transfer of one atomic layer to the top of another[16]. However, the atomic layers involved have to be prepared in advance by epitaxial growth, mechanical exfoliation[22], liquid-phase exfoliation[23,24] or chemical vapor deposition (CVD)[25–27], making this approach quite complicated. In addition, the achievement in rational stacking between atomic layers is still challenging for the atomic layer transfer strategy. Recently, a templating CVD method has been developed, realizing the epitaxial growth of graphene on *h*-BN, ZnO and ZnS[28,29]. Although the quality of the atomic-scale heterostructures is guaranteed, the CVD reactions had to be stimulated through a plasma or arc-discharge treatment and expensive, complicated instruments had to be used. The growth of MoS_2 on graphene was also reported through a hydrothermal method[30], but it is not feasible to use such a method to generate high quality atomic layer heterostructures because the formation of nanoparticles is more favorable than atomic layers for MoS_2 under hydrothermal conditions. Thus, the development of a simple, controllable, and cost-effective method for the fabrication of large-area, high-quality atomic multilayered heterostructures with superb properties is highly desirable.

Herein, we describe a transfer-free method for the preparation of large-area, high-quality multilayered graphene/MoS_2 heterostructured films in a controlled manner. The films have been fabricated through an *in situ* catalytic process by simply heating Mo-oleate complex coated on sodium sulfate particles under a N_2 atmosphere. Taking advantage of the greatly shortened lithium ion diffusion distance and the outstanding electronic conductivity, the graphene/MoS_2 heterostructured films exhibit high specific capacity, excellent rate performance and cycling stability, even at high current densities, when used as an anode material for lithium batteries.

The preparation procedure of graphene/MoS_2 heterostructured films is provided in Supplementary Fig. S1. First, Mo-oleate was obtained by aging the mixture of molybdenum pentachloride ($MoCl_5$), sodium oleate and a small amount of de-ionized water at 358 K for 3 h. The Mo-oleate formed was uniformly coated on the surface of

sodium sulfate particles and then transferred to a tube furnace and heated in a N_2 atmosphere. After the product was washed with de-ionized water and dried at 353 K, graphene/MoS_2 heterostructured films were obtained.

For the preparation of large-area uniform graphene/MoS_2 heterostructures, sodium sulfate single crystals were used as a substrate and a source of sulfur, while Mo-oleate complex as the sources of Mo and carbon. 2D atomic crystals usually grow on flat substrates and the nature of substrates gives an important impact on the quality of the 2D atomic crystals generated. The substrates with inactive surfaces such as SiO_2 film function only as flat supports for the growth of atomic layers[31], while the metal-based substrates, such as Cu[32], Ni[33] or Ru[34], not only work as supports but also prompt the formation of atomic layers. However, the removal of the metal substrates usually caused contamination of the formed layers by metal impurities. For the preparation of graphene/MoS_2 heterostructures, we chose sodium sulfate crystals as a substrate. In addition to the smooth crystal facets which provide an ideal support for the growth of the heterostructures, sodium sulfate solid functions as a sulfur source for the generation of MoS_2 through a local CVD reaction. More importantly, the sodium sulfate substrate can be easily removed to generate free-standing atomic layers by washing with de-ionized water after the reactions.

A proposed formation mechanism for the graphene/MoS_2 heterostructured films is illustrated in Fig. 1 and the possible chemical reactions are listed in Supplementary Equations. Upon stirring sodium sulfate crystals with pre-prepared Mo-oleate gently, a uniform Mo-oleate ultrathin layer was coated on the surface of sodium sulfate particles (Fig. 1a). After heated at high temperature in a N_2 atmosphere, amorphous carbon thin films are formed through carbonization of the coating molybdenum oleate complex on the surface of sodium sulfate particles. The amorphous carbon thin films would reduce sulfate on the surface of the sulfate particles to form Na_2S, and the hydrolysis of Na_2S leads to the formation of hydrogen sulfur. A local CVD reaction was expected to take place to generate uniform MoS_2 atomic layer through the reaction of hydrogen sulfur with Mo species, resulting in an amorphous carbon/MoS_2 film supported on the surface of the remaining sodium sulfate crystals was obtained (Fig. 1b). Transmission electron microscopy (TEM) and the selected area electron diffraction (SAED) of the amorphous carbon/MoS_2 films prepared by heating at 873 K for 0.5 h are shown in Fig. S2. From the TEM image, it is seen that the amorphous carbon/MoS_2 films are rather uniform. The SAED pattern of the films shows one set of six-fold symmetry diffraction spots and diffraction rings, ascribed to MoS_2 crystal and the amorphous carbon, respectively. The SAED pattern demonstrates the existence of crystalline MoS_2 and amorphous carbon species in the films generated. Compared with traditional CVD methods using external H_2S or S as a source of sulfur[31,35], this local CVD process is simple in producing uniform MoS_2 atomic layer.

Further heating the reactant for 3 h in a N_2 atmosphere leads to growth of graphene on MoS_2 through the conversion of the amorphous carbon, generating graphene/MoS_2 heterostructures on the surface of sodium sulfate (Fig. 1c). The scanning electron microscopy (SEM) image shows that the coated film has a lateral size of >140 μm (Fig. S3). After removal of Na_2SO_4 substrate by simply washing with de-ionized water, an ultrathin graphene/MoS_2 heterastructured film was obtained (Fig. 1d–e). The uniformity and high quality of the heterostructured film are well demonstrated by the TEM observation (Fig. 2a). The SAED pattern of the film shows one set of strong single crystal diffraction spots (labeled in white color) and another set of weak single crystal spots (labeled in yellow color), attributing to the crystalline MoS_2 and few-layered graphene, respectively (Fig. 2b). The X-ray photoelectron spectra (XPS) technique has been used to further identify the nature of carbon in the heterostructured films (Fig. S4). The C 1 s XPS spectra show a main peak near 284.5 eV, ascribed to the sp^2-hybridized carbon[36]. The presence of the sp^2-hybridized carbon indicates the catalytic growth of graphene on MoS_2 layer from the amorphous carbon. The high-resolution TEM observation at the edge of the film obviously shows the stacking of MoS_2 layer on the top of graphene atomic layer (Fig. 2c). From the analyses of the AFM and the corresponding height profiles (Fig. 2d–g), the thicknesses of individual graphene and MoS_2 layers are measured to be approximately 1.6 and 1.2 nm, respectively. This result might suggest that the heterostructured film consists of a carbon layer composed of four single graphene sheets and one single MoS_2 sheet. To further prove the existence of both graphene and MoS_2, we performed the large area spatially Raman mapping (532 nm), collecting spectra on a 15 × 30 μm grid with 6 × 6 spots. The Raman spectra are shown in Figure S5 a–d and the E^1_{2g}, A^1_g, D and G peaks intensities of the spectra are plotted as maps, respectively. From the Raman mapping images of E^1_{2g}, A^1_g, D and G intensities (Figure S5 e–h), the characteristic peaks of E^1_{2g} and A^1_g for MoS_2, and those of D and G for graphene are detected in each spot of the selected large-area region of our material, revealing the growth of large area graphene/MoS_2 heterostruture in our material. Moreover, the scanning transmission electron microscopy (STEM) technique was also used to identify the elemental distribution of carbon, sulfur and Mo in a film. The STEM image of GM1 is shown in Figure S6. It exhibits uniform distribution of carbon, sulfur and

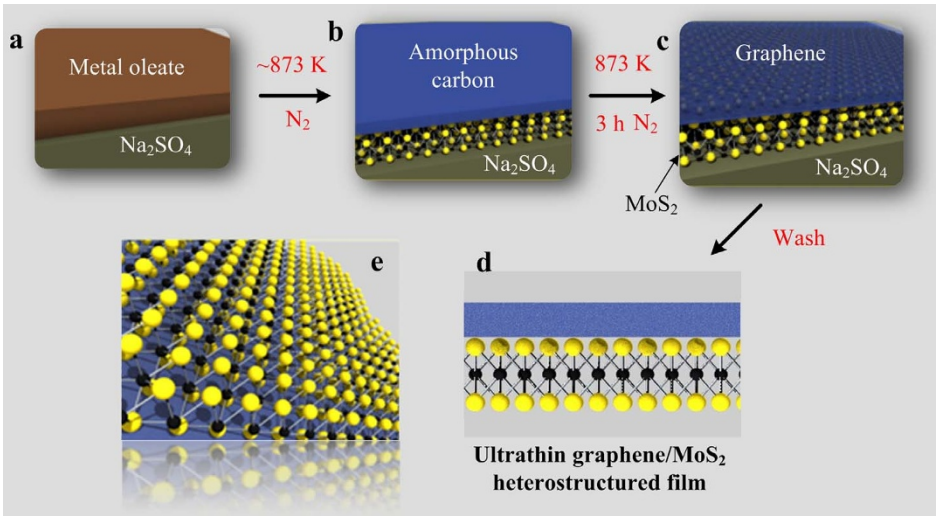

Figure 1 | Schematic representation of the preparation procedure and formation mechanism of multilayered graphene/MoS_2 heterostructure.

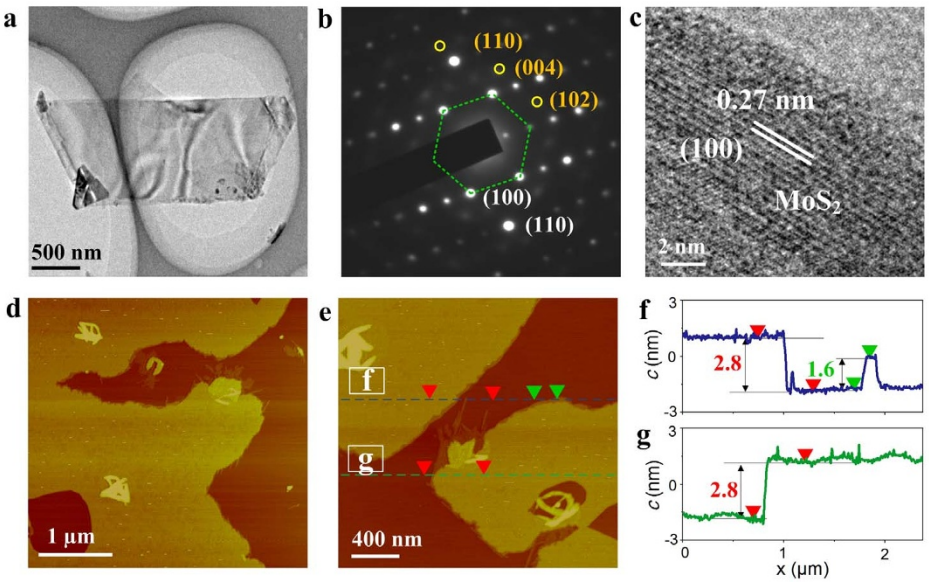

Figure 2 | General characterization of multilayered graphene/MoS_2 of heterostructures. (a) TEM image and (b) the SAED pattern, indicating that the heterostructured film consists of a crystalline MoS_2 and graphene sheets with the hexagonal structures (white and yellow colors correspond to the crystal planes related to the diffraction spots of MoS_2 and graphene species, respectively). (c) High-resolution TEM image, showing the stacking of MoS_2 sheet on graphene. (d–e) AFM images and (f–g) the corresponding height profiles along the dashed lines of e, demonstrating the thicknesses of the MoS_2 and graphene layers.

Mo in the film, revealing the existance of 2D heterostructure of graphene and MoS_2.

To reveal the nature of graphene layers catalytically grown on MoS_2 more clearly, we removed the MoS_2 layer from the heterostructured film using strong acids. The TEM image shows that the remaining ultrathin film is quite large and uniform (Fig. 3a). The related EDX analysis shows that only carbon element is present in the film, indicating that the MoS_2 layer has been removed completely (Fig. S7). The SAED pattern (Inset of Fig. 3a) of the carbon film presents a hexagonal symmetry of graphene. The AFM image (Fig. 3b) and the corresponding height profile (Inset of Fig. 3b) shows that the thickness of the graphene film is approximately 1.66 nm, in good agreement with that of the graphene/MoS_2 heterostructured films.

It is believed that the MoS_2 atomic layers function as both a template and a catalyst during the formation of the graphene. The growth of large-area graphene is catalyzed by the *in situ* formed MoS_2 hexagonal atomic crystals. Under intense conditions graphene has also been prepared on hexagonal atomic layers previously[37,38,29]. Employed graphite flake as carbon source and ZnO or ZnS as catalysts, Liu *et al*[29] obtained graphene sheets by using an arc-discharge method. Yang *et al*[37] reported the epitaxial growth of graphene on *h*-BN by breaking down the methane with a remote plasma source. A catalyst-free transformation of amorphous carbon into graphene via current-induced annealing was reported by Barreiro *et al*[38]. It is worth noting that for the growth of large-area graphene on the MoS_2 layer, no external forces are involved, making our *in situ* catalytic process simple and environmentally friendly.

The number of MoS_2 sheets in the graphene/MoS_2 heterostructured films can be controlled by varying the molar ratio of $MoCl_5$ to sodium oleate. When the molar ratio is 1 : 5, the heterostructured film, denoted as GM1 is mainly composed of one MoS_2 sheet and one graphene layer (Fig. 2). Increasing the molar ratio to 2 : 5, the heterostructured film, denoted as GM2, mainly contains three MoS_2 sheets (Fig. S8 a,b). Further increasing the molar ratio to 4 : 5, the number of MoS_2 sheets in the heterostructured film, denoted as GM3, is mainly six (Fig. S8 c,d). In the AFM images, the thickness of a heterostructured film measured is approximately 2.7 and 5.6 nm for the samples GM2 and GM3, respectively, consistent with the results of the high-resolution TEM observation. Interestingly, in GM2 and GM3, the interlayer distance between adjacent single-layer MoS_2 is approximately 1.0 nm, equal to the sum of $d(002)$ spacing of MoS_2 (0.62 nm) and the thickness of single-carbon layer (0.34 nm). Furthermore, the Raman spectrum was used to identify the nature of single-carbon layer. It shows two sharp G and 2D bands at around 1576 and 2686 cm^{-1} respectively, revealing that the interlayer carbon might

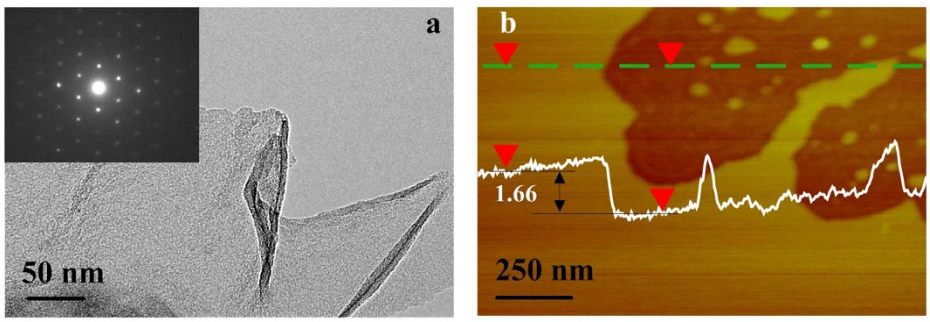

Figure 3 | Identification of the nature of the carbon layer in graphene/MoS_2 heterostructure. (a) TEM image and the inserted SAED pattern of the carbon layer obtained through removal of the MoS2 layer from the heterostructured film. (b) AFM image and the inserted height profile.

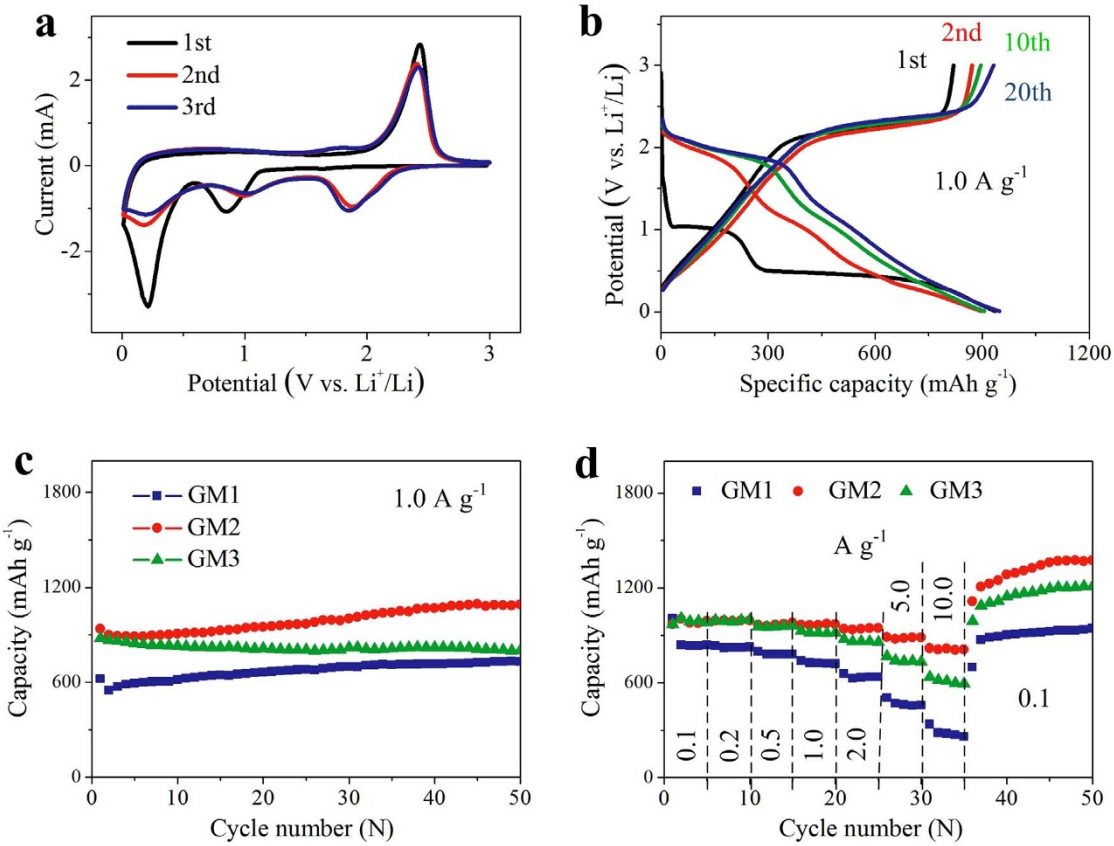

Figure 4 | Battery performance of GM1, GM2 and GM3. (a) Cyclic voltammogrames of GM2 at a scanning rate of 1.0 mV s^{-1}. (b) Galvanostatic charge-discharge profiles of GM2 at 1.0 A g^{-1}. (c) Cycling performance at high current density of 1.0 A g^{-1}. (d) Rate performance at various current densities of 0.1, 0.2, 0.5, 1.0, 2.0, 5.0 and 10.0 A g^{-1}.

be graphene (Fig. S9). The possible synthesis mechanism for heterostructures with different number of MoS_2 sheets (as illustrated in Fig. S10) is that the increase in sheet number of MoS_2 with molar ratio of $MoCl_5$ might be due to increased number of MoO_x sheets derived from the hydrolysis of $MoCl_5$. The subsequent local CVD reaction of these MoO_x sheets with hydrogen sulfur generates the corresponding MoS_2 sheets.

As a typical 2D chalcogenide, atomic layered MoS_2 is promising for use as an electrode material in rechargeable lithium ion batteries due to the large specific capacity and high rate performance[6,39–41]. However, the poor electronic/ionic conductivity between two adjacent S-Mo-S layers still limits their further applications[42]. Furthermore, the lithiation product Li_2S is prone to reacting with the electrolyte to produce a thick gel-like polymeric layer, which leads to the capacity fading and inferior rate capability[43,44]. It is expected that these issues can be resolved by switching to the multi-layered graphene/MoS_2 heterostructures, in which atomic layers of MoS_2 are coated with graphene to enhance the electronic/ionic conductivity and to reduce the reactions at the interface between MoS_2 atomic layer and electrolyte[45,46].

In this work, the electrochemical performance of the graphene/MoS_2 heterostructured films has been evaluated as an electrode material for lithium-ion batteries. The initial three consecutive cyclic voltammograms (CVs) of the three MoS_2-layered films are shown in Fig. 4a. There are two cathodic peaks located at 0.87 and 0.22 V in the first cycle. The peak at 0.87 V corresponds to the intercalation of Li^+ into the MoS_2 lattice to form Li_xMoS_2. The other peak at 0.22 V is attributed to the decomposition of MoS_2 into Mo nanoparticles following the reaction, $MoS_2 + 4Li^+ + 4e^- \rightarrow Mo + 2Li_2S$. The Mo nanoparticles generated are embedded in a Li_2S matrix. In the reverse anodic curve, a very small oxidation peak at 1.77 V is detected, attributed to the partial oxidation of Mo into MoS_2. The distinct peak located at 2.43 V is ascribed to the conversion of Li_2S into S. After the first cycle, the electrode is mainly composed of Mo and S instead of the initial MoS_2. In the following cycles, the cathodic peaks at around 1.83, 1.0 and 0.2 V are ascribed to the formation of Li_2S, Li_xMoS_2, and Mo, respectively, as illustrated in equations (1–3). The CV curves with distinct redox peaks are consistent with those reported in the literature for MoS_2 materials[47–49]. Stable redox peaks for the conversion between Li_2S and S are clearly observed upon cycling, indicating that the stability of the heterostructured films upon lithiation and delithiation. The graphene sheets in the heterostructured films not only improve the electronic conductivity, but also prevent the dissolution of intermediate lithium polysulfide products, ensuring the cycling stability.

$$2Li^+ + S + 2e^- \rightarrow Li_2S \quad (1)$$

$$MoS_2 + xLi^+ \rightarrow Li_xMoS_2 \quad (2)$$

$$Li_xMoS_2 + (4-x)Li^+ + (4-x)e^- \rightarrow Mo + 2Li_2S \quad (3)$$

Figure 4b shows galvanostatic discharge/charge profiles of the graphene/MoS_2 heterostructured films at a high current density of 1.0 A g^{-1} in the voltage range of 0.01 ~ 3.0 V (vs. Li^+/Li). In the initial discharge process, two potential plateaus at about 1.0 and 0.5 V are observed, attributed to the formation of Li_xMoS_2 and the decomposition of MoS_2, in consistence with CV results. In the following discharge processes, two potential plateaus at about 1.9 and 1.2 V are

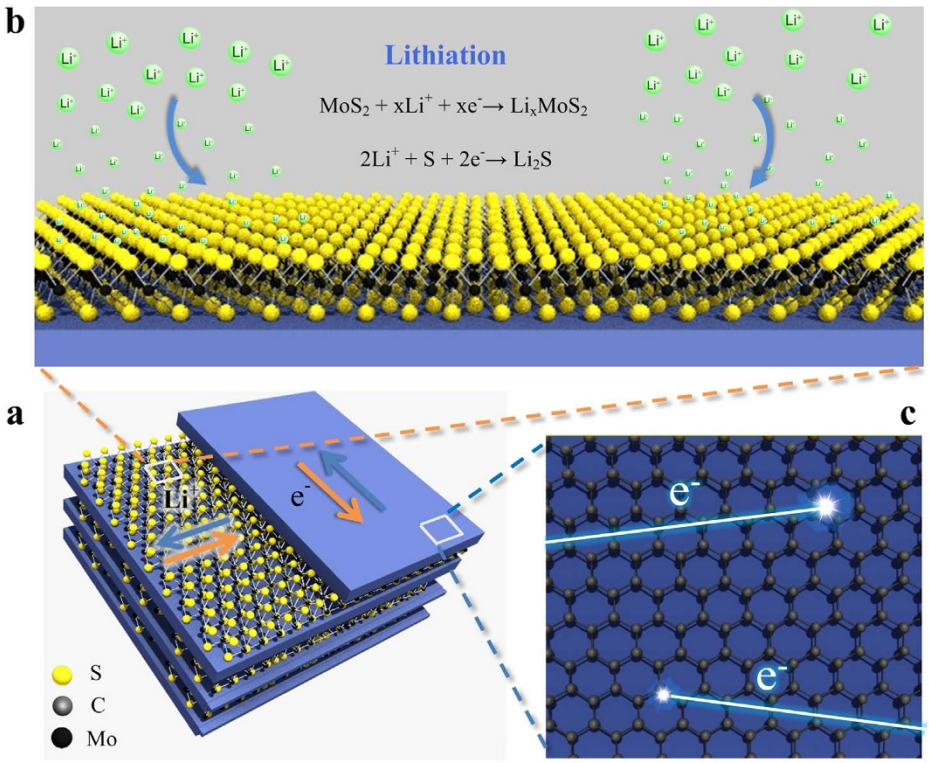

Figure 5 | Schematic representation of diffusions of Li^+ and electron in GM2 during charge and discharge processes. (a) The multilayered graphene/MoS_2 heterostructures. (b) The diffusion of Li ions into the heterostructured film from the front and side surfaces of MoS_2 layers. (c) The electron conduction in the graphene layer. These graphene/MoS_2 heterostructured films enhance the high contact area, shorten the Li ion diffusion length and promote the faster transfer of electrons in the material.

observed, corresponding to the formation of Li_2S and Li_xMoS_2, respectively, upon lithium ion insertion. The distinct plateau at approximately 2.3 V in the charge profiles is ascribed to the generation of S upon the Li^+ extraction. The negligible variation of this plateau upon cycling indicates that insertion and extraction of lithium ion in and from S is highly reversible. The initial discharge and charge capacities of the MoS_2-layered films are 936 and 820 mAh g^{-1}, respectively, giving a coulombic efficiency of 88%. The irreversible capacity of approximately 116 mAh g^{-1} is due to the formation of solid electrolyte interface (SEI) film, decomposition of electrolyte, and reduction of oxygen-containing groups[50]. The coulombic efficiency increases to over 99% in the subsequent cycles. Compared with the MoS_2-based electrode materials reported in the literature[45–50], the heterostructured films show distinctly high coulombic efficiency and large capacities at high current densities, attributing to the unique heterostructure of these graphene/MoS_2 thin films.

The variation of the specific charge capacities of the graphene/MoS_2 heterostructured films are plotted as a function of cycling number (Fig. 4c). The cycling performance of the heterostructured films GM1, GM2, and GM3 is tested at a current density of 1.0 A g^{-1}. A slight increase in the charge capacity with charge/discharge cycles is observed for both GM1 and GM2, attributed to the gradual activation of the electrode upon lithiation and delithiation. Large discharge capacities of approximately 1100, 800, and 730 mAh g^{-1} are retained for the GM2, GM3, and GM1, respectively after 50 cycles, distinctly higher than those presented in the literature (580 mAh g^{-1})[49,51]. Compared with GM1 and GM3, GM2 exhibits the highest charge capacity and the best cycling stability. In addition to the remarkable cycleability, the heterostructures also exhibit excellent rate performance. Figure 4d shows the variations of the reversible capacities with current densities and discharge-charge cycles. The cells were first cycled at 0.1 A g^{-1} for 5 cycles, followed by cycling at current densities increasing stepwise to as high as 10 A g^{-1}. Compared with GM1 and GM3, GM2 exhibits superior rate performance. For GM2, a reversible capacity of approximately 990 mA h g^{-1} is achieved at a current density of 0.1 A g^{-1}, 970 mAh g^{-1} at 0.5 A g^{-1}, 930 mAh g^{-1} at 2.0 A g^{-1}, and 820 mAh g^{-1} at 10.0 A g^{-1}. Cycled at 10.0 A g^{-1}, reversible capacities of 269 and 606 mAh g^{-1} are obtained for GM1 and GM3, respectively, much lower than that of GM2. Decreasing the current density back to 0.1 A g^{-1} after cycling at 10.0 A g^{-1}, reversible capacities of 920, 1360, and 1202 mAh g^{-1} are restored for GM1, GM2, and GM3, respectively, indicating the good reversibility and structural stability of these heterostructured films. To the best of our knowledge, such a remarkably high electrochemical performance has never been reported so far for MoS_2 materials in the literature.

The electrochemical performance of MoS_2-based heterostructured films depends on the film thickness and the weight of MoS_2 content in a hybrid active material. GM1 has the highest content of graphene in the composite, while GM3 shows the highest conent of MoS_2 in the composite (Table S1). However, as shown in Fig. 4, GM2 exhibits the highest charge capacity and the best cycling stability. The superb electrochemical performance of GM2 is ascribed to its appropriate mass ratio of graphene/MoS_2 in the composite. The appropriate MoS_2 content in GM2 ensures the high specific capacity of the electrode, while the thin graphene layers improve the electronic conductivity of the electrode and ensure the cycling stability of S generated electrochemically.

It is believed that the high capacity and excellent rate performance is associated with the unique multilayered graphene/MoS_2 heterostructures. As demonstrated by the schematic illustration in Fig. 5, the graphene/MoS_2 heterostructure is composed of appropriate number of graphene and MoS_2 atomic layers, ensuring the structure stability and facilitating the transport of electrons and the diffusion of lithium ions (Fig. 5a). Due to the small thickness of the films, the Li^+ ions may get sufficient contact with the atomic layers of MoS_2 (Fig. 5b). The interlayered graphene not only improves the electronic

conductivity, but also prevent the adverse reactions at the interface between MoS_2 and electrolyte, and the dissolution of intermediate lithium polysulfide products (Fig. 5c). As a result, excellent electrochemical performance is achieved for graphene/MoS_2 heterostructured films.

We have synthesized large-area multilayered graphene/MoS_2 heterostructures with a tunable sheet number through *in situ* catalytic growth of graphene on MoS_2 atomic crystal. The uniform heterostructured films exhibit excellent electrochemical performance when used as an electrode material for LIBs. For the heterostructure with mainly three MoS_2 sheets, large discharge capacities of approximately 1100 mA g^{-1} are delivered at a current density of 1.0 A g^{-1} for 50 cycles. Taking advantage of uniformity, large area, and high electronic quality, these heterostructured films may find use in more traditional fields such as electronics or catalysis. This simple, controllable, and inexpensive synthetic strategy is also applicable for the preparation of other multilayered graphene/metal sulfide heterostructures with attractive properties.

Methods

Materials. All the reagents for synthesis and preparation were of analytic grade and used as received without further purification. Molybdenum pentachloride were purchased from Acros. Sodium oleate and sodium sulfate were purchased from TCI and Aldrich, respectively.

Preparation of graphene/MoS_2 heterostructures. In a typical procedure, a certain amount of molybdenum pentachloride ($MoCl_5$, Acros) was dissolved in 2.0 mL of de-ionized water and then mixed with 1.22 g sodium oleate (TCI, 95%).The mixture was aged at 358 K for 3 h, leading to the formation of molybdenum oleate. 10.0 g of sodium sulfate (Aldrich, 98%) was mixed well with the above molybdenum oleate by grounding. During this process, molybdenum oleate was uniformly coated on the surface of sodium sulfate particles. The ground mixture was heated at 873 K with a ramping rate of 10 K min^{-1} under a N_2 atmosphere for 3 h. After cooled down naturally, the product was washed with de-ionized water to remove unreacted sodium sulfate and then dried at 353 K for 12 h. In order to control the number of MoS_2 layers, the molar ratios of $MoCl_5$ to sodium oleate were chosen to be 1 : 5, 2 : 5 and 4 : 5, and the corresponding products are denoted GM1, GM2 and GM 3, respectively.

General characterization. The transmission electron microscopy (TEM) images were taken with a JEM-2100Fmicroscope operated at an acceleration voltage of 200 kV. The scanning electron microscopic (SEM) images were obtained with a FEI Nova NanoSEM 2300. The Raman spectra were obtained by using a Senterra Raman spectrometer (Bruker AG). XPS measurements were conducted on a Kratos Axis Ultra DLD spectrometer using a monochromated Al Kα radiation. The atomic force microscope (AFM) images were taken on a Multimode-NanoscopeIIIa microscope (Digital Instrument).

The battery performance. The working electrode was fabricated as follows. First, the MoS_2 (70 wt%), Super-P carbon black (15 wt%, Timcal), and sodium carboxymethyl cellulose (15 wt%) were mixed in an ethanol/water solution to form a slurry. The slurry was spread onto a Cu foil by a doctor blade method, followed by drying in vacuum at 343 K for 8 h. A lithium foil acted as both the counter and reference electrodes, and a microporous polypropylene membrane (Celgard 2500) was used as the separator. CR2016 coin cells were assembled in an argon-filled glove box with both moisture and oxygen contents below 1.0 ppm. The electrolyte was 1.0 M $LiPF_6$ in the mixture of ethylene carbonate (EC) and dimethyl carbonate (DMC) (1 : 1 in volume ratio). The galvanostatic charge and discharge experiment was performed with a battery tester LAND-CT2001A in the voltage range of 0.01 $\sim$ 3.0 V at room temperature. The cyclic voltammetry was conducted on a CHI660B electrochemical workstation at a scanning rate of 1.0 mV/s in a potential range of 0.01 $\sim$ 3.0 V (vs. Li/Li^+).

1. Geim, A. K. & Grigorieva, I. V. Van der Waals heterostructures. *Nature* **499**, 419–425 (2013).
2. Novoselov, K. S. *et al.* Two-dimensional atomic crystals. *Proc. Natl Acad. Sci. USA* **102**, 10451–10453 (2005).
3. Britnell, L. *et al.* Field-effect tunneling transistor based on vertical graphene heterostructures. *Science* **335**, 947–950 (2012).
4. Levendorf, M. P. *et al.* Graphene and boron nitride lateral heterostructures for atomically thin circuitry. *Nature* **488**, 627–632 (2012).
5. Lee, C. *et al.* Frictional characteristics of atomically thin sheets. *Science* **328**, 76–80 (2010).
6. Coleman, J. N. *et al.* Two-dimensional nanosheets produced by liquid exfoliation of layered materials. *Science* **331**, 568–571 (2011).
7. Ye, J. *et al.* Accessing the transport properties of graphene and its multilayers at high carrier density. *Proc. Natl Acad. Sci. USA* **108**, 13002–13006 (2011).
8. Li, Y. *et al.* MoS_2 nanoparticles grown on graphene: An advanced catalyst for the hydrogen evolution reaction. *J. Am. Chem. Soc.* **133**, 7296–7299 (2011).
9. Son, M., Lim, H., Hong, M. & Choi, H. C. Direct growth of graphene pad on exfoliated hexagonal boron nitride surface. *Nanoscale* **3**, 3089–3093 (2011).
10. Ding, X., Ding, G., Xie, X., Huang, F. & Jiang, M. Direct growth of few layer graphene on hexagonal boron nitride by chemical vapor deposition. *Carbon* **49**, 2522–2525 (2011).
11. Wang, Q. H., Kalantar-Zadeh, K., Kis, A., Coleman, J. N. & Strano, M. S. Electronics and optoelectronics of two-dimensional transition metal dichalcogenides. *Nature Nanotech.* **7**, 699–712 (2012).
12. Sup Choi, M. *et al.* Controlled charge trapping by molybdenum disulphide and graphene in ultrathin heterostructured memory devices. *Nature Commun.* **4**, 1624 (2013).
13. Dean, C. R. *et al.* Boron nitride substrates for high-quality graphene electronics. *Nature Nanotech.* **5**, 722–726 (2010).
14. Yankowitz, M. *et al.* Emergence of superlattice Dirac points in graphene on hexagonal boron nitride. *Nature Phys.* **8**, 382–386 (2012).
15. Ci, L. *et al.* Atomic layers of hybridized boron nitride and graphene domains. *Nature Mater.* **9**, 430–435 (2010).
16. Xue, J. *et al.* Scanning tunnelling microscopy and spectroscopy of ultra-flat graphene on hexagonal boron nitride. *Nature Mater.* **10**, 282–285 (2011).
17. Britnell, L. *et al.* Strong light-matter interactions in heterostructures of atomically thin films. *Science* **340**, 1311–1314 (2013).
18. Fang, H. *et al.* Quantum of optical absorption in two-dimensional semiconductors. *Proc. Natl Acad. Sci. USA* **110**, 11688–11691 (2013).
19. Osada, M. & Sasaki, T. Two-dimensional dielectric nanosheets: novel nanoelectronics from nanocrystal building blocks. *Adv. Mater.* **24**, 210–228 (2012).
20. Xu, M., Liang, T., Shi, M. & Chen, H. Graphene-like two-dimensional materials. *Chem. Rev.* **113**, 3766–3798 (2013).
21. Wei, D. *et al.* Scalable synthesis of few-layer graphene ribbons with controlled morphologies by a template method and their applications in nanoelectromechanical switches. *J. Am. Chem. Soc.* **131**, 11147–11154 (2009).
22. Novoselov, K. S. *et al.* Electric field effect in atomically thin carbon films. *Science* **306**, 666–669 (2004).
23. Hernandez, Y. *et al.* High-yield production of graphene by liquid-phase exfoliation of graphite. *Nature Nanotech.* **3**, 563–568 (2008).
24. Stankovich, S. *et al.* Synthesis of graphene-based nanosheets via chemical reduction of exfoliated graphite oxide. *Carbon* **45**, 1558–1565 (2007).
25. Kim, K. S. *et al.* Large-scale pattern growth of graphene films for stretchable transparent electrodes. *Nature* **457**, 706–710 (2009).
26. Berger, C. *et al.* Electronic confinement and coherence in patterned epitaxial graphene. *Science* **312**, 1191–1196 (2006).
27. Li, X. *et al.* Large-area synthesis of high-quality and uniform graphene films on copper foils. *Science* **324**, 1312–1314 (2009).
28. Dai, B. *et al.* Rational design of a binary metal alloy for chemical vapour deposition growth of uniform single-layer graphene. *Nature Commun.* **2**, 522 (2011).
29. Huang, L. *et al.* Gram-scale synthesis of graphene sheets by a catalytic arc-discharge method. *Small* **9**, 1330–1335 (2013).
30. Koroteev, V. O. *et al.* Charge transfer in the MoS_2/carbon nanotube composite. *J. Phys. Chm. C* **115**, 21199–21204 (2011).
31. Wang, X., Feng, H., Wu, Y. & Jiao, L. Controlled synthesis of highly crystalline MoS_2 flakes by chemical vapor deposition. *J. Am. Chem. Soc.* **135**, 5304–5307 (2013).
32. Yan, K., Fu, L., Peng, H. & Liu, Z. Designed CVD growth of graphene via process engineering. *Acc. Chem. Res.*, **46**, 2263–2274 (2013).
33. Yu, Q. *et al.* Graphene segregated on Ni surfaces and transferred to insulators. *Appl. Phys. Lett.* **93**, 113103 (2008).
34. Sutter, P. W., Flege, J.-I. & Sutter, E. A. Epitaxial graphene on ruthenium. *Nature Mater.* **7**, 406–411 (2008).
35. Zhuo, S., Xu, Y., Zhao, W., Zhang, J. & Zhang, B. Hierarchical nanosheet-based MoS_2 nanotubes fabricated by an anion-exchange reaction of MoO_3–amine hybrid nanowires. *Angew. Chem. Int. Ed.* **125**, 8764–8768 (2013).
36. Lin, T.-W., Liu, C.-J. & Lin, J.-Y. Facile synthesis of MoS_3/carbon nanotube nanocomposite with high catalytic activity toward hydrogen evolution reaction. *Appl. Catal. B-environ.* **134–135**, 75–82 (2013).
37. Yang, W. *et al.* Epitaxial growth of single-domain graphene on hexagonal boron nitride. *Nature Mater.* **12**, 792–797 (2013).
38. Barreiro, A. *et al.* Understanding the catalyst-free transformation of amorphous carbon into graphene by current-induced annealing. *Sci. Rep.* **3**, 1115 (2013).
39. Ramakrishna Matte, H. S. S. *et al.* MoS_2 and WS_2 analogues of graphene. *Angew. Chem. Int. Ed.* **49**, 4059–4062 (2010).
40. Hwang, H., Kim, H. & Cho, J. MoS_2 nanoplates consisting of disordered graphene-like layers for high rate lithium battery anode materials. *Nano Lett.* **11**, 4826–4830 (2011).
41. Ding, S., Chen, J. S. & Lou, X. W. Glucose-assisted growth of MoS_2 nanosheets on CNT backbone for improved lithium storage properties. *Chem. – Eur. J.* **17**, 13142–13145 (2011).
42. Laursen, A. B., Kegnaes, S., Dahl, S. & Chorkendorff, I. Molybdenum sulfides-efficient and viable materials for electro - and photoelectrocatalytic hydrogen evolution. *Energ. Environ. Sci.* **5**, 5577–5591 (2012).

43. Zheng, G. *et al*. Amphiphilic surface modification of hollow carbon nanofibers for improved cycle life of lithium sulfur batteries. *Nano Lett.* **13**, 1265–1270 (2013).
44. Yang, Y. *et al*. High-capacity micrometer-sized Li_2S particles as cathode materials for advanced rechargeable lithium-ion batteries. *J. Am. Chem. Soc.* **134**, 15387–15394 (2012).
45. Hassoun, J. & Scrosati, B. A high-performance polymer tin sulfur lithium ion battery. *Angew. Chem. Int. Ed.* **49**, 2371–2374 (2010).
46. Armand, M. & Tarascon, J. M. Building better batteries. *Nature* **451**, 652–657 (2008).
47. Yu, H. *et al.* Three-dimensional hierarchical architectures constructed by graphene/MoS_2 nanoflake arrays and their rapid charging/discharging properties as lithium-ion battery anodes. *Chem. – Eur. J.* **19**, 5818–5823 (2013).
48. Gong, Y. *et al*. A bottom-up approach to build 3D architectures from nanosheets for superior lithium storage. *Adv. Funct. Mater.* **24**, 125–130 (2014).
49. Yang, L. *et al*. Hierarchical MoS_2/polyaniline nanowires with excellent electrochemical performance for lithium-ion batteries. *Adv. Mater.* **25**, 1180–1184 (2012).
50. Rout, C. S. *et al*. Synthesis and characterization of patronite form of vanadium sulfide on graphitic layer. *J. Am. Chem. Soc.* **135**, 8720–8725 (2013).
51. Wang, Z. *et al*. CTAB-assisted synthesis of single-layer MoS_2-graphene composites as anode materials of Li-ion batteries. *J. Mater. Chem. A* **1**, 2202–2210 (2013).

Acknowledgments

This work was financially supported by the National Basic Research Program of China (2013CB934102, 2011CB808703) and the National Natural Science Foundation. The authors greatly thank Dr. Yongli Zheng for her kindly help in Raman mapping measurement.

Author contributions

W.F. and K.X.W. developed the idea and designed the experiments. W.F. performed the sample fabrication, measurements and data analysis. F.H.D. performed the electrochemical experiments. W.F., K.X.W., F.H.D., X.H.L., X.W., T.N.Y., J.S. and J.S.C. analyzed the data, and discussed the results. W.F., K.X.W. and J.S.C. co-wrote the paper. J.S.C. planned and supervised the project.

Additional information

Supplementary information accompanies this paper at http://www.nature.com/scientificreports

Competing financial interests: The authors declare no competing financial interests.

How to cite this article: Fu, W. *et al. In situ* catalytic growth of large-area multilayered graphene/MoS_2 heterostructures. *Sci. Rep.* **4**, 4673; DOI:10.1038/srep04673 (2014).